

Synthesis of zero-valent Cu nanoparticles in the chitosan coating layer on cellulose microfibrils: evaluation of azo dyes catalytic reduction

Tahseen Kamal · Sher Bahadar Khan ·
Abdullah M. Asiri

Received: 25 January 2016 / Accepted: 20 March 2016 / Published online: 4 April 2016
© Springer Science+Business Media Dordrecht 2016

Abstract A facile, fast, and economically viable method has been used to synthesize highly active copper (Cu) nanoparticles in chitosan (CH) coating layers over cellulose microfibrils of filter paper (FP). FP was coated with 1 wt% CH solution (CH-FP) and kept in CuSO_4 aqueous solution to adsorb Cu^{2+} ions. The Cu^{2+} loaded CH-FP was treated with 0.1 M NaBH_4 aqueous solution to reduce the ions to Cu^0 nanoparticles. The Cu^0 loaded CH-FP (Cu/CH-FP) was characterized by FE-SEM, XRD, TGA and ATR-FTIR, which indicated the successful preparation of the Cu^0 nanoparticles by this method. The crystallinity of cellulose was not affected during the preparation process, which indicated that the Cu^0 nanoparticles were present in the amorphous thin CH layer around the cellulose microfibrils of FP. The Cu/CH-FP was used in aqueous medium as an efficient catalyst for the reduction of toxic organic dyes. Our current study

involved the degradation of methyl orange (MO) and Congo red (CR) dyes in the presence of NaBH_4 . The rate constants of 0.2683 and 0.1655 min^{-1} were observed for the MO and CR reductions. Besides good catalytic activity, the Cu/CH-FP catalyst strip could be easily recovered as compared to the other methods that are currently used. Recovery was accomplished by simply pulling the Cu/CH-FP strip from the reaction medium after completion of the reaction. The recovered Cu/CH-FP could be recycled several times provided that its exposure time to the air was minimal.

Keywords Cu^0 nanoparticles · Chitosan · Cellulose filter paper · Catalyst · Dye reduction

Electronic supplementary material The online version of this article (doi:10.1007/s10570-016-0919-9) contains supplementary material, which is available to authorized users.

T. Kamal (✉) · S. B. Khan · A. M. Asiri
Center of Excellence for Advanced Materials Research (CEAMR), King Abdulaziz University,
P.O. Box 80203, Jeddah 21589, Saudi Arabia
e-mail: tkkhan@kau.edu.sa

T. Kamal · S. B. Khan · A. M. Asiri
Department of Chemistry, Faculty of Science, King
Abdulaziz University, P.O. Box 80203, Jeddah 21589,
Saudi Arabia

Introduction

Metallic nanoparticles have attracted increasing attention in recent years because of their applications in variety of fields, i.e., bio-imaging, sensing, drug delivery, antimicrobial coating and so on (Ahmad et al. 2015; Ghodake et al. 2016; Moritz and Geszke-Moritz 2013; Nie et al. 2010; Pezzato et al. 2015; Sapsford et al. 2013). Besides the above common applications, they are extensively utilized as catalysts in a wide variety of chemical reactions such as hydrogen liberation (Caliskan et al. 2012), Suzuki cross-coupling (Fihri et al. 2011), hydrocarbon

oxidation (Zhang et al. 2011), ring opening (Shen et al. 2013) and phenolic derivative upgradation reactions (Sarkar et al. 2014). Metallic nanoparticles possess high activity originating from their high surface-to-volume ratio due to the small sizes. There are two main hurdles associated with the usage of metal nanoparticles as catalyst. First, nanoparticles readily form aggregates because of van der Waals forces, and preventing their agglomerate formation is difficult. Such agglomeration of nanoparticles results in a decrease of surface area; hence, the catalytic activity drops (Zahmakran and Ozkar 2011). Second, nanoparticle separation after completion of reactions is difficult because of their small size (Carino et al. 2009). Scientists have aimed their efforts to overcoming the above-mentioned hurdles. A single solution to agglomerate prevention and easy recycling was to use catalyst supports. The utilization of catalyst support has two-fold advantages. First, they improve the stability and dispersability (Yan et al. 2004). Second, as a hosting material, the separation and reuse of catalysts from the reaction system become easy (Baig and Varma 2013). Generally, catalyst supports for metallic nanoparticles are either inorganic [e.g., silica (Li et al. 2013), carbon (Cordier et al. 2010), metal oxide (Yan et al. 2004)] or organic materials (Guo et al. 2014). Organic supports are better than inorganic as they have a few advantages such as versatility (they can be easily functionalized) and chemical inertness (no interference with the catalyst) (Guo et al. 2014). Commonly used organic supports are micrometer- or submicrometer-sized beads made of polymethyl methacrylate spheres, which were reported for the immobilization of palladium nanoparticles (Song and Yi 2008). Chen and Chen (1998) fabricated Pt-coated polystyrene microspheres by a wet chemistry approach for the hydrogenation of allyl alcohol in water. Polymer single crystals were used by Li et al. (Dong et al. 2012) as high surface area support for immobilization of Pt nanoparticles. Similarly, some recent approaches have used other high surface area polymeric supports such as poly(acrylic acid)/poly(vinyl alcohol) nanofibers (Xiao et al. 2012) and cellulose nanocrystals (Johnson et al. 2011; Zhou et al. 2013) for loading of noble metal nanoparticles, etc. Cellulose in the form of filter paper (FP) was also used for loading of Au nanoparticles and was demonstrated as an easily recoverable dip catalyst (Zheng

et al. 2015). As alternatives to noble metal nanoparticles, transition metal nanoparticles have proven to be similar or a few have claimed them to be more enhanced catalytic activities (Datta et al. 2014; Zhou et al. 2013). Along with the fascinating properties of the organic supports, sometimes they need special and longer procedures for their preparation. For instance, poly(ϵ -caprolactone) macromolecules must be synthesized with –HS functional groups instead of –OH for the effective loading of the nanoparticles (Dong et al. 2012). Furthermore, most of the support materials have been designed and synthesized, adding steps to the preparation of catalyst (Song and Yi 2008; Xiao et al. 2012). Therefore, support materials with readily availability are highly desirable.

Within the past few years, synthetic polymer-based catalyst supports were prepared, and catalytic activities of various transition metal nanoparticles were tested (Sahiner 2013). They explored hydrogels as good supports for catalysts in aquatic chemical reactions because the reactant molecules can easily approach the catalyst surface (Sahiner et al. 2010, 2011). However, hydrogels are soft and break during handling. Therefore, a hydrogel coated onto a high surface area yet mechanically strong support is highly desirable for use as a catalytic support. To avoid the long procedures for the designing and synthesis of new materials, we relied on abundantly available natural resources such as cellulose (Eta and Mikkola 2016; Zhong et al. 2016) and chitosan (chitin derivative) (González et al. 2015) as catalytic support.

In this article, we prepared Cu/CH-FP (FP-filter paper as a high surface area cellulose support) catalyst for effective and economical water treatment. The Cu/CH-FP was made by a CH aqueous solution coating on FP, adsorption of Cu^{2+} ions from CuSO_4 aqueous solution followed by adsorbed Cu^{2+} ions to Cu^0 nanoparticles via treating the samples with NaBH_4 solution. In this study, the prepared samples were characterized by FT-IR, XRD and SEM. The actual amount of Cu nanoparticles was estimated by thermogravimetric analysis. The application of Cu/CH-FP was studied in methyl orange (MO) and Congo red (CR) dye degradation in their aqueous solutions. This novel Cu/CH-FP has great potential for use as an economical, environmentally friendly, easily recyclable and sustainable catalyst.

Experimental

Materials

Chitosan in the yellowish powdered form was purchased from Sigma-Aldrich. Sodium borohydride (NaBH_4 , 99 %), acetic acid and copper sulfate ($\text{CuSO}_4 \cdot 7\text{H}_2\text{O}$, 99 %) were purchased from BDH chemicals. Methyl orange and Congo red dyes were obtained from Koch-lite Laboratories, UK. Cellulose filter papers (12.5 cm diameter and 0.3 mm thickness) were purchased from Whatman Co. All products were of analytical grade and used without further purification; 18.2 $\text{M}\Omega$ cm water was obtained from a Millipore system and used throughout this work.

Catalyst preparation

The following two-step procedure was adopted for the easy preparation of catalyst:

1. Chitosan (CH) solution with a concentration of 1 % w/v was prepared in dilute acetic acid aqueous solution (10 % v/v) at room temperature with stirring overnight. It was then coated on a cellulose microfiber mat by dipping it in CH solution and whipping out the excess solution. Typically, $0.6 \times 4.5 \text{ cm}^2$ of CH-FP was cut and used for the in situ preparation of the Cu metal nanoparticles.
2. Copper nanoparticles were prepared inside CH layers on FP by adsorption of Cu^{2+} ions followed by their reduction. FP with a known weight was treated with CH solution (1 wt% in 10 % acetic acid solution). CH-FP was dipped and kept in 50 ml 0.1 M $\text{CuSO}_4 \cdot 7\text{H}_2\text{O}$ aqueous solution for the adsorption and loading of the Cu^{2+} ions. The strip was left for 2 h in Cu^{2+} aqueous solution to saturate the adsorption sites. It was then gently washed with DI water, introduced into 50 ml of NaBH_4 aqueous solution (0.8 M) and kept for 2 h to completely reduce the Cu^{2+} ions to Cu nanoparticles. After this step, the Cu nanoparticle-loaded CH-FP (Cu/CH-FP) was washed with DI water and freshly used in further experiments.

Evaluation of catalytic property

The catalytic activity of the Cu/CH-FP was evaluated in the MO and CR dye reductions using NaBH_4 . We used a

glass UV cuvette as reaction vessel. Three solutions of NaBH_4 , MO and CR dyes were prepared with concentrations of 0.1 M, 0.003 mM and 0.012 mM in DI water, respectively. Next we explain the catalytic behavior of Cu/CH-FP in MO reduction by NaBH_4 . To a UV cuvette, 4 ml of MO dye solution and 0.3 ml of NaBH_4 aqueous were introduced, and UV-visible spectra were recorded by a UV-visible spectrophotometer (Evolution 300). After this, a $0.6 \times 4.5 \text{ cm}^2$ Cu/CH-FP strip was introduced in such a way that the film normal was pointing at the translucent sides of the cuvette while keeping the path free for the UV-visible light in the spectrophotometer to pass through it. The reduction reaction was initiated as soon as Cu/CH-FP was added to the cuvette. The variation in absorbance value at 464 nm for MO was noted and compared with the previously constructed calibration curve. The Cu/CH-FP was easily taken out of the cuvette by just pulling its strip and used again for the MO dye degradation. The reusability experiments were performed after washing the Cu/CH-FP three times with DI water and used again for MO dye reduction reactions. It is important to note that all the catalytic experiments were performed one after another so that the Cu/CH-FP had less chance to get oxidized by air. A similar procedure was adopted for the CR dye degradation experiments.

Characterization

The morphology of the samples was characterized by field emission scanning electron microscope (FE-SEM) with a JEOL JSM-7600F, Japan. Samples were stuck with carbon tape onto a 1-cm-diameter stub and coated with Pt prior to SEM observations. Crystal structures of samples were analyzed by performing X-ray diffraction (XRD) on a PANalytical diffractometer with $\text{Cu-K}\alpha$ radiation ($\lambda = 0.154 \text{ nm}$) source. The instrument was operated at 40 kV and 50 mA, and data were obtained at a scan rate of $2^\circ 2\theta \text{ min}^{-1}$. The percentage crystallinity (Cr %) of bare FP, CH-FP and Cu/CH-FP samples was calculated from the XRD patterns using the following equation:

$$\text{Cr (\%)} = \frac{I_{(200)} - I_{\text{amorphous}}}{I_{(200)}} \times 100 \quad (1)$$

where $I_{(200)}$ and $I_{\text{amorphous}}$ represent the intensity of the (200) peak and intensity of the amorphous halo, respectively. For cellulose I, the intensity of diffraction at $2\theta = 18^\circ$ was chosen as the $I_{\text{amorphous}}$.

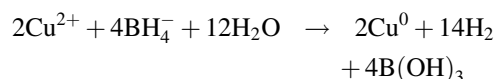
Crystallite sizes of Cu nanoparticles and cellulose were calculated using the following Scherrer formula,

$$\tau = \frac{K\lambda}{\beta \cos \theta} \quad (2)$$

where τ , λ , β and θ are respectively the crystallite size, wavelength of X-rays, full width of the peak at half maximum (FWHM) and the scattering angle of the peak. FWHM was calculated from XRD patterns by Fityk software. Fourier transform infrared (FT-IR) spectra were recorded in the range of 400–4000 cm^{-1} on a PerkinElmer (spectrum100) ATR-FT-IR spectrometer. Thermogravimetric analysis was performed on 10 mg of sample using a TGA Q500 instrument. Samples were placed in aluminium pans and kept on the autosampler stage of the TGA instrument. Their weight lost against temperature was recorded under nitrogen atmosphere with a 10 $^{\circ}\text{C}/\text{min}$ heating rate up to 600 $^{\circ}\text{C}$. The residual concentrations of MO and CR dyes in catalytic reduction studies were measured using a Thermo Scientific Evolution 300 UV-visible spectrophotometer.

Results and discussions

Figure 1 shows the schematic illustration of the steps involved in the Cu/CH-FP. CH coating of the FP resulted in a slightly brittle and mechanically strong CH-FP as compare to the bare FP because of connecting the individual cellulose microfibers by CH polymer. The color of CH-FP changed from white to the light blue after treating the CH-FP with CuSO_4 aqueous solution, which confirmed the Cu^{2+} ion uptake by the thin CH layer. The formation of Cu nanoparticles during the dipping process of the Cu^{2+} -loaded CH-FP into NaBH_4 aqueous solution was followed by the strip color change of blue to black. It took just 3 min for the color change, indicating the reaction was quite fast. The proposed reaction for this process is given as follows:



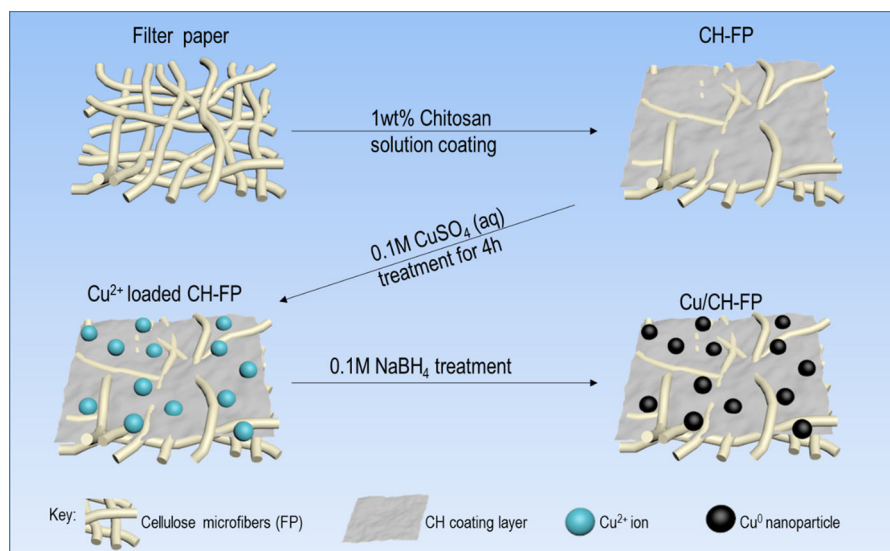
The successful preparation of Cu^0 nanoparticles depends on the quality of the water. Water de-oxygenated by a bubbling NaBH_4 aqueous solution with inert gases or nitrogen has been used in

previously reported methods to avoid metal oxide formation (Hudson et al. 2012; Smuleac et al. 2011). The hydrogen gas released in the above reaction also protects the Cu^0 nanoparticles against their oxidation. We have, however, used freshly generated DI water where the chance of dissolved oxygen is low.

Figure 2 represents FE-SEM images of the materials studied in this investigation. FP was composed of cellulose microfibers (Fig. 2a). The size of microfibers falls between 10 and 16 μm . The FP also had nanofibrils in addition to microfibers, as indicated by the arrows in the image (Fig. 2a). The hierarchically fibrous network structure of FP was retained after a coating of 1 wt% CH solution, as shown in Fig. 2b. There was no obvious change in the morphology of the original FP surface. In fact, coating of FP with a denser CH solution results in a thick film formation, which was not suitable here (see Supporting Information Figure SI 1) (Kamal et al. 2015). The cellulose fiber surface in CH-FP was smooth, indicating that the CH was uniformly coated. However, a significant morphological difference can be observed on nanometer scale for the Cu/CH-FP. As can be clearly seen from the FE-SEM image in Fig. 2c, plenty of bright spots were regularly distributed on the microfibers. These bright spots were due to the Cu nanoparticles present in the CH coating layer while the original hierarchical fibrous morphology was retained. Figure 2d represents the EDX spectrum of the selected area highlighted with a pink rectangle in Fig. 2c. A distinct peak of Cu validates the presence of nanoparticles in the sample where most of the sample was composed of the carbon and oxygen of the FP cellulose.

XRD patterns of FP, CH-FP and Cu/CH-FP are shown in Fig. 3. The FP pattern has peaks at $2\theta = 14.8^{\circ}$, 16.2° , 22.5° and 34.3° corresponding to the $(\bar{1}10)$, (110) , (200) and (004) planes of the cellulose I. The XRD patterns of CH-FP and Cu/CH-FP were identical to the FP, suggesting that all the samples had crystalline cellulose content and CH was only amorphously adsorbed on the FP. The cellulose crystal information of the crystallinity and crystallite size is given in Table 1. The cellulose crystallinities in CH-FP and Cu/CH-FP were similar to the bare FP, and the crystallite size did not change. Figure 3c represents the XRD pattern of Cu/CH-FP. In addition to the major reflections from cellulose, three more reflections at $2\theta = 43.7^{\circ}$, 50.4° and 73.9° were observed,

Fig. 1 Schematic illustration of the Cu/CH-FP preparation

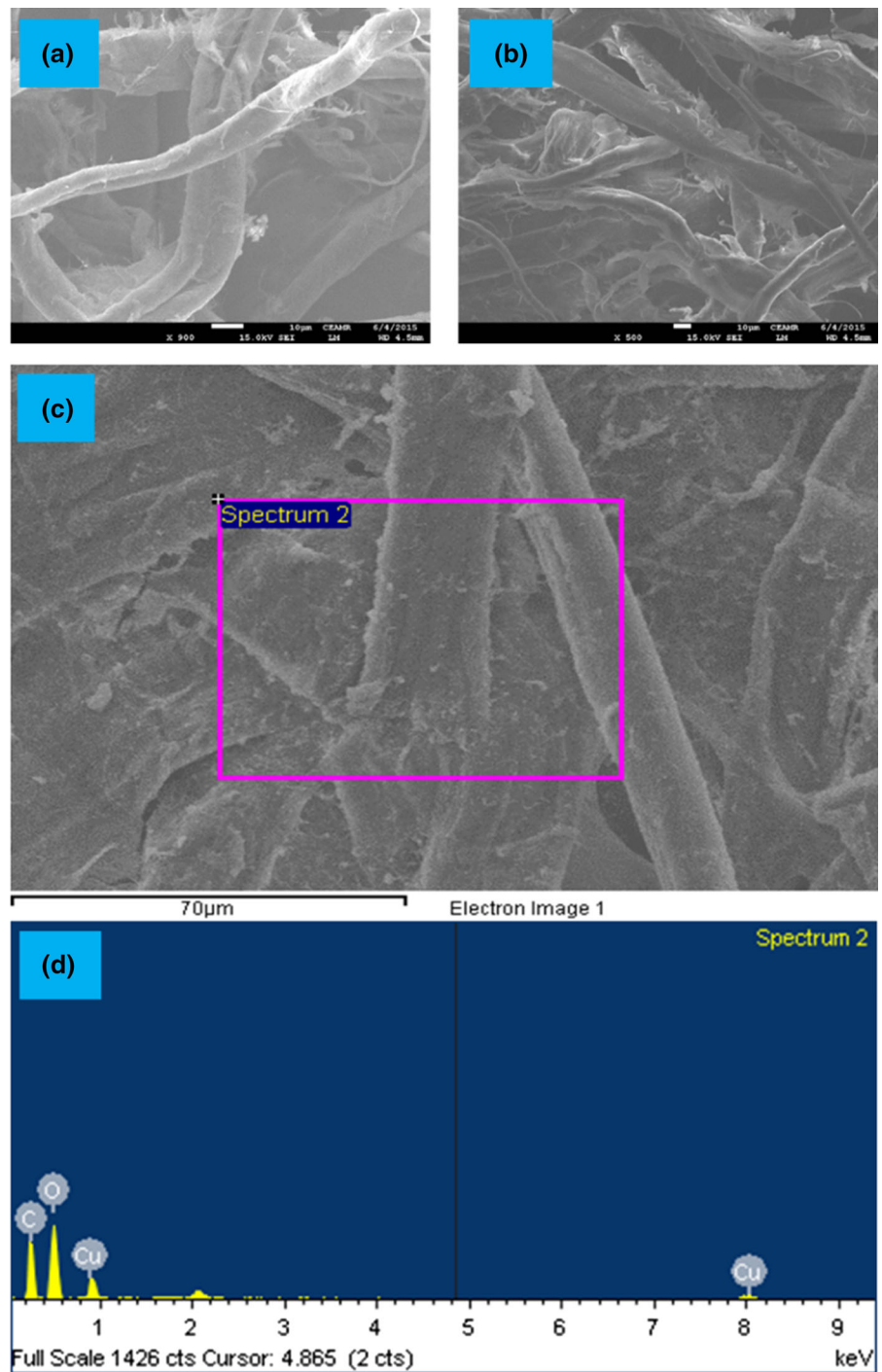


which corresponded to the (111), (200) and (220) crystalline planes of the Cu^0 [JCPDS 4-0836 (FCC Cu)]. This emphasizes that the Cu^0 nanoparticles were successfully synthesized in the CH layer.

Figure 4 shows the ATR-FTIR spectra of FP, CH-FP and Cu/CH-FP. The two spectra of CH-FP and Cu/CH-FP were identical to those of the FP spectrum. The FP spectrum showed a typical FTIR of cellulose, which was extensively discussed in terms of peak assignment in previous reports (Abidi et al. 2014; Oh et al. 2005). No shifting of peaks was observed in the Cu/CH-FP. This was due to the low content of the prepared Cu nanoparticles and hence failure of this technique. However, the crystalline fractions were computed by comparing the relative intensities of specific peaks in the CH-FP and Cu/CH-FP. The crystallinity of cellulose was estimated through a parameter known as the lateral order index (LOI), which is defined as the ratio of the intensity of the peak at 1426 cm^{-1} to the peak at 898 cm^{-1} (Kljun et al. 2011). The obtained LOI values of 0.51 and 0.52 for CH-FP and Cu/CH-FP were similar to each other, suggesting that FP processing for CH coating and Cu nanoparticle preparation did not alter the crystallinity of the cellulose. Such an observation is important because the mechanical properties of the semi-crystalline polymers depend on the crystalline fraction. These results suggest that Cu/CH-FP might have similar strong mechanical properties of the cellulose.

Figure 5 shows the TGA thermograms of CH-FP and Cu/CH-FP. A first mass loss of around 10 % near $100\text{ }^\circ\text{C}$ for both samples was observed. This reduction in mass was due to the moisture loss. The next mass loss for CH-FP occurred between 250 and $370\text{ }^\circ\text{C}$ because of the depolymerization, oxidation and evolution of gases. Compared to other reports on the addition of inorganic nanofillers, which raises the thermal stability of polymers [12–20], a lowering of this degradation temperature for Cu/CH-FP was observed. Such a lowering of the degradation temperature for Cu/CH-FP was due to the catalytic nature of Cu nanoparticles, which decreased the activation energy and lifted the depolymerization reaction. Thermal decomposition temperature data deduced from the TGA experiments on CH-FP and Cu/CH-FP are shown in Table 2. This table displays the initiation of the thermal decomposition temperature at which the cellulose starts to decompose (T_{onset}), the temperature at which the degradation reaction rate reaches its maximum (T_{max}) and the decomposition end temperature (T_{end}) at which the degradation reaction finishes. It is clear from Table 1 that T_{onset} , T_{max} and T_{end} were slightly lower for Cu/CH-FP than CH-FP. Another objective of the thermal analysis was to determine the amount of Cu nanoparticles present in the Cu/CH-FP. The difference between the two thermograms at $600\text{ }^\circ\text{C}$ was 6.1 %, which suggests that 20 mg of Cu/CH-FP contained $1.4 \pm 0.5\text{ mg}$ of Cu nanoparticles.

Fig. 2 FE-SEM images of **a** FP, **b** CH-FP and **c** Cu/CH-FP. The EDX spectrum **d** of the selected area in **c**



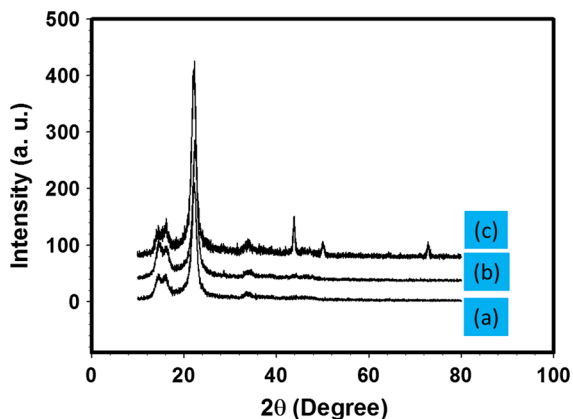


Fig. 3 XRD patterns of *a* FP, *b* CH-CH-FP and *c* Cu/CH-FP

Table 1 Structural parameters of FP, CH-FP and Cu/CH-FP

Sample ID	Crystal size (nm)	Crystallinity (%)	LOI ^b
FP	6.97	78	0.51
CH-FP	6.97	79	0.51
Cu/CH-FP	6.84/18 ^a	78	0.52

^a For Cu nanoparticles

^b Determined by ATR-FTIR

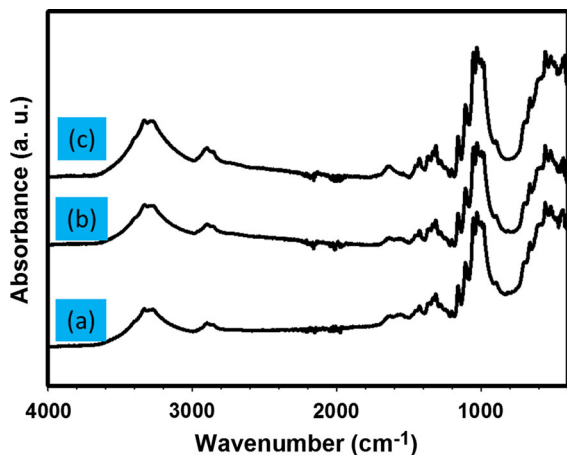


Fig. 4 ATR-FTIR spectra of *a* FP, *b* CH-FP and *c* Cu/CH-FP

Evaluation of catalyst in chemical reactions

MO dye reduction

The degradation of organic dyes by the excess of NaBH₄ in the presence of catalyst is widely used to analyze the catalytic properties of various catalysts.

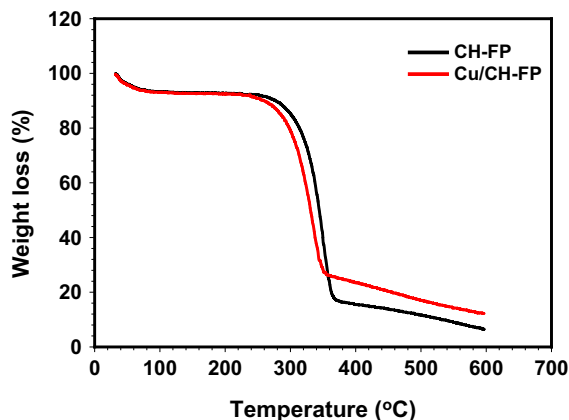


Fig. 5 TGA thermograms of CH-FP and Cu/CH-FP

Herein, we choose the MO reduction by NaBH₄ in the presence of Cu/CH-FP catalyst. This reduction reaction is thermodynamically favorable but kinetically unfavorable (Rehman et al. 2015). MO is widely used in industries and academic institutes as a pH indicator whose chemical structure contains an azo group. There are several environmental and health-related problems due to which its degradation is of great interest (Chauhan and Mohanty 2015).

MO imparts an orange-red color to the solution when dissolved in water at pH 7. Its aqueous solution results in strong absorption of visible light at 464 nm and one weak absorption at 264 nm. The absorption at 464 nm is due to the presence of the –N=N– functional group in the MO chemical structure. It is well known that the reduction of MO by NaBH₄ is kinetically slow in the absence of suitable catalyst. Previous reports suggest that the peak intensity at 464 nm remains constant for several hours when a reaction is carried out without using any catalyst (Khan et al. 2014a). Such an observation suggests that this reaction is not kinetically favorable and could not proceed by utilizing only NaBH₄ and skipping the use of catalyst (Rehman et al. 2015). Since our catalyst, Cu/CH-FP, consisted of around 94 % non-metallic support (CH-FP), we first incorporated a CH-FP strip to a UV cuvette containing 4 ml of 0.003 mM MO dye and 0.3 ml of NaBH₄. UV-visible spectral data were continuously recorded with a 1-min interval between measurements. The results of this experiment are shown in Fig. 6a. The peak maxima at 282 and 464 nm decreased to a very small extent. However, this small decrease in the intensity of both peaks can

Table 2 Important parameters deduced from TGA analysis of CH-FP and Cu/CH-FP

Samples	T_{onset} (°C)	T_{max} (°C)	T_{end} (°C)	Wt loss at 600 °C (%)
CH-FP	220	349	367	9
Cu/CH-FP	201	335	351	15.1

not be considered due to the degradation of MO. Instead, MO can be adsorbed on the high surface cellulose microfibers of CH-FP. This result is in line with our recent report (Kamal et al. 2015). Figure 6b shows the UV-visible absorption spectra of the MO solution where Cu/CH-FP was introduced. The peak intensity at 464 nm decreased gradually with time and the peak at 282 shifted slightly and reached 250 nm while its intensity increased. The digital photographs of this experiment are shown in Figure SI 2. The gradual disappearance of peak at 464 nm with the introduction of Cu/CH-FP was due to the initiation of the MO degradation reaction, which was completed in the short time of 13 min. NaBH_4 reduces MO at the $-\text{N}=\text{N}-$ site and produces low molecular amino compounds. Therefore, the new peak appearance at 250 nm was considered from the $-\text{NH}_2$ compound formation during the MO reduction (Khan et al. 2014a). Although MO dye was reduced in 13 min, it could be reduced faster if Cu/CH-FP was suspended in the solution. This is because, in the present experiment, only one side of Cu/CH-FP was in contact with the MO solution in the UV cuvette, while the other side was along the walls of the container (Figure SII). Figure 6c shows the degradation percentage of MO by NaBH_4 in the presence of CH-FP and Cu/CH-FP. The degradation percentage

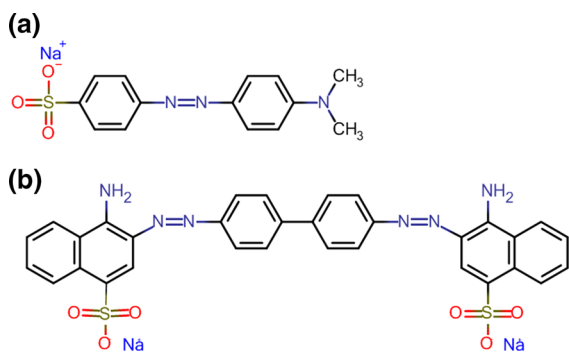
was calculated from the UV-visible spectra of MO as follows:

$$\text{Degradation percentage} = 100 - (A_t \times 100/A_0) \quad (3)$$

where A_0 and A_t relate to the initial absorbance and absorbance (λ_{max} , in the present case 464 nm) at time t during the reaction, respectively. As discussed earlier, NaBH_4 was unable to reduce the MO in the presence of CH-FP. Instead, around 6 % MO dye was adsorbed on the CH-FP surface. The 100 % degradation of MO by NaBH_4 in the presence of Cu/CH-FP was completed within just 13 min. Figure 6c represents the plots of A_t/A_0 as a function of time for CH-FP and Cu/CH-FP. The ratio of A_t/A_0 for Cu/CH-FP decreased clearly compared to CH-FP. This indicates the superior catalytic performance of Cu/CH-FP over using CH-FP.

Congo red dye reduction

Another notorious dye for water contamination is CR [1-naphthalenesulfonic acid, 3,3'-(4,4'-biphenylenebis(azo))bis(4-amino-)disodium salt]. CR reduction was selected as a model reaction because it is a pollutant that is associated with carcinogenicity and causes great harm to aquatic environments. CR is a benzidine-based anionic azo dye known to metabolize benzidine, a human carcinogen (Afkhani and Moosavi 2010). The aromatic structure of CR is responsible for its physicochemical, thermal and optical stability (Gautam et al. 2015). Thus, it is necessary to remove such toxic dyes from wastewater before it is discharged into aquatic environments. The CR chemical structure consists of two azo groups (Fig. 6). It was previously observed in the HPLC and LC-MS analysis of the products that the reduction of azo dyes leads to cleavage of the $-\text{N}=\text{N}-$ bond (Patel and Suresh 2006; Plum et al. 2003). As a result of this cleavage, aromatic amines are formed. Keeping this in mind, we expected a slower reduction reaction of CR because it has two $-\text{N}=\text{N}-$ groups per molecule.

**Fig. 6** Chemical structures of MO and CR

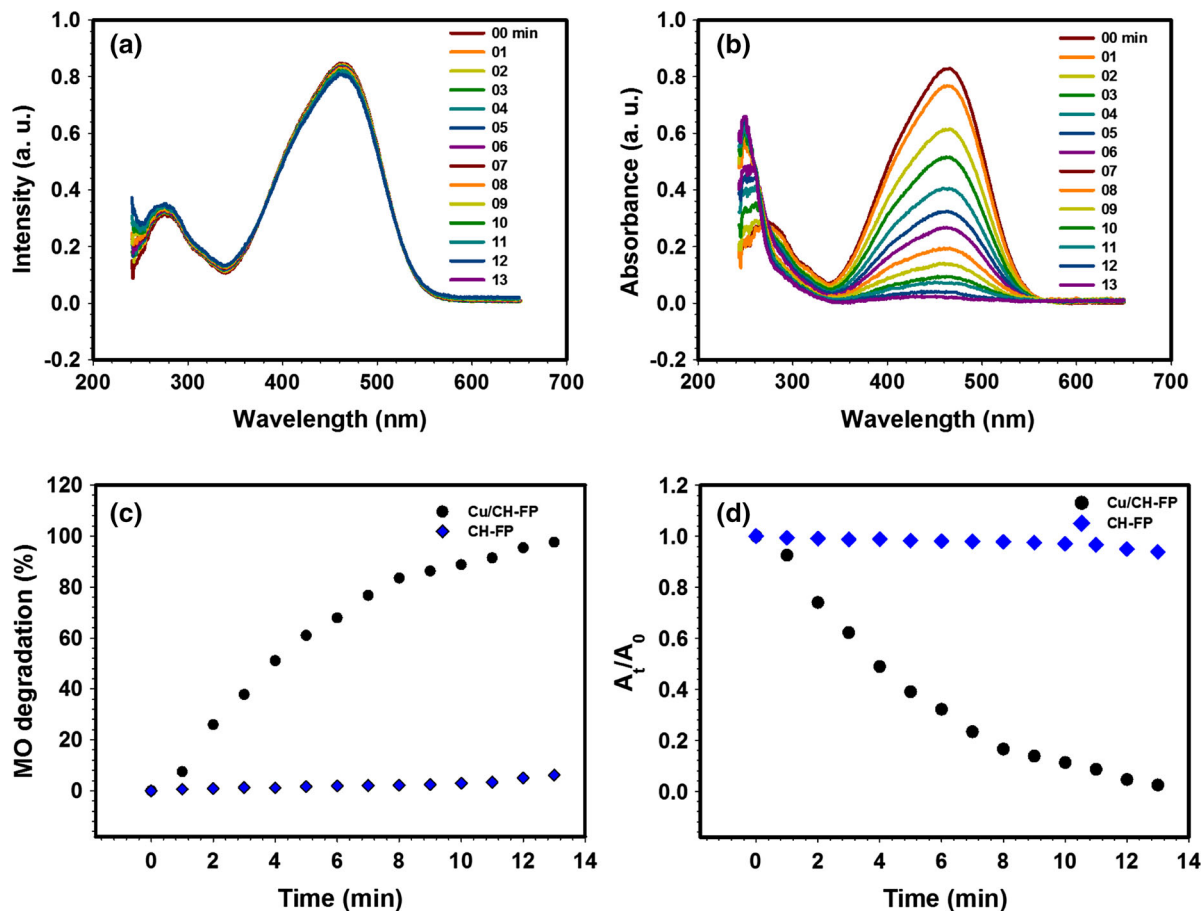


Fig. 7 Absorbance spectra of MO aqueous solution at different intervals of time where **a** CH-FP and **b** Cu/CH-FP strips were used as catalysts. MO degradation percentage (**c**) and A_t/A_0 (**d**) plots as functions of time for CH-FP and Cu/CH-FP.

Experimental conditions: $0.6 \times 4.5 \text{ cm}^2$ strips of CH-FP or Cu/CH-FP, 4 ml of 0.003 mM MO aqueous solution and 0.3 ml of 0.1 M NaBH_4 aqueous solution

Just like previous experiments, we used CH-FP in a cuvette containing CR and NaBH_4 , and the solution UV-visible spectra were monitored with a regular and constant interval of time. Figure 8a shows the successive UV-visible spectra of the solution containing CH-FP. There were two peaks at 438 nm and 592 nm due to CR in the solution. The absorbance at $\lambda_{\text{max}} = 592 \text{ nm}$ changed slightly with time, which could be considered due to the CR adsorption on the CH-FP during this time. Figure 8b shows the UV-visible spectra of the CR solution at constant intervals between measurements where Cu/CH-FP was used to catalyze the reduction reaction by NaBH_4 . The digital photographs of this experiment are shown in Figure SI 3. A clear decrease in the absorbance of both peaks can be seen with time. Moreover, with time, a

new peak evolved at 290 nm. Such changes in the UV-visible spectra suggest that the original CR molecules degraded by NaBH_4 into smaller ones upon using Cu/CH-FP. Figure 8c represents the reduction percentages of CR as functions of time. CR reduction was negligibly small in the presence of CH-FP, whereas it was completely reduced in the presence of Cu/CH-FP. Similarly, the plots of A_t/A_0 as functions of time for CH-FP and Cu/CH-FP are shown in Fig. 8c, which reaches similar results as discussed above.

It was clear from the results of the experiments on MO and CR that the Cu^0 nanoparticles were mainly responsible for their catalytic reduction. Furthermore, the data in Figs. 7d and 8d were fitted with a linear correlation using the following equation (Khan et al. 2014b):

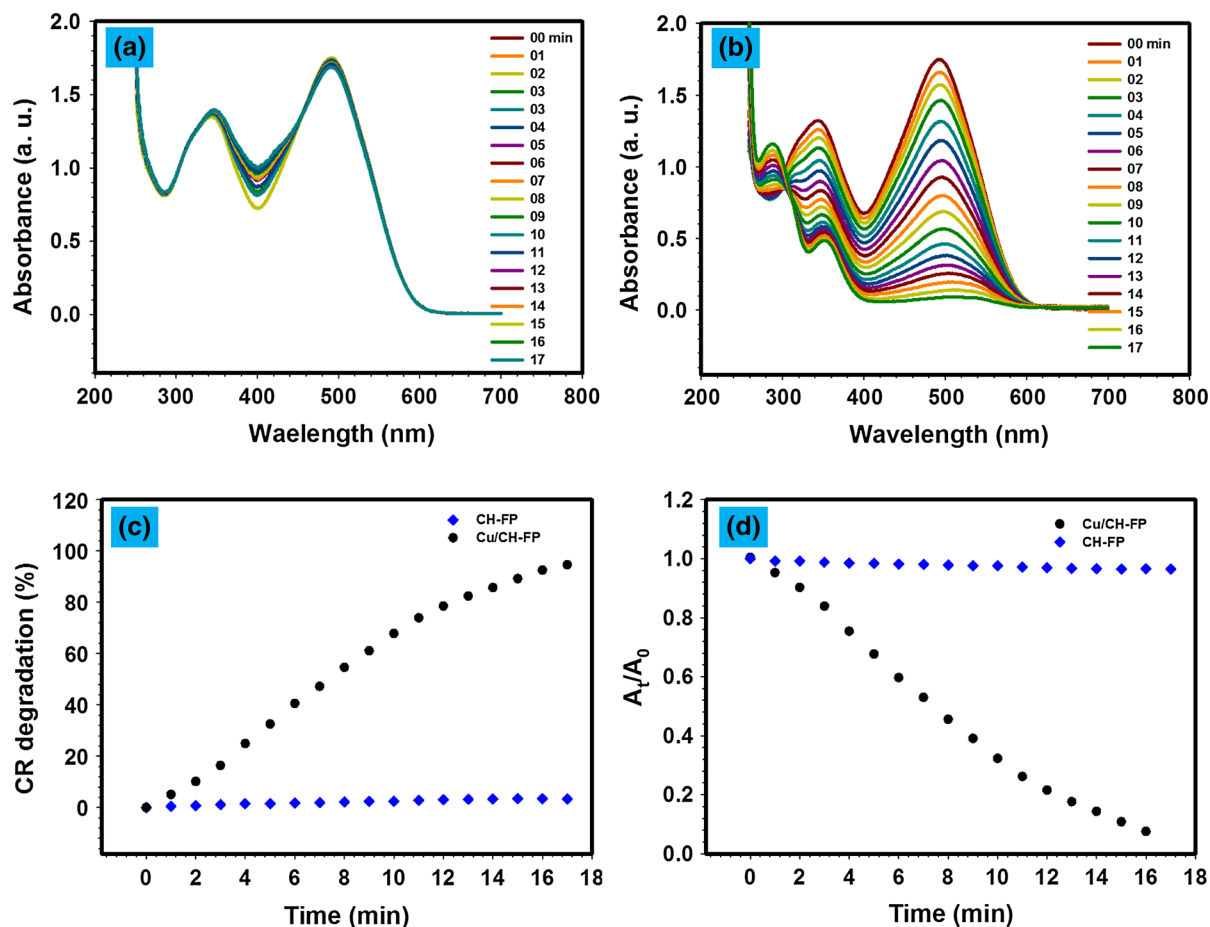


Fig. 8 Absorbance spectra of CR aqueous solutions for **a** CH-FP and **b** Cu/CH-FP at different intervals of time. CR degradation percentage (c) and A_t/A_0 (d) plots as functions of time for CH-FP

and Cu/CH-FP. Experimental conditions: $0.6 \times 4.5 \text{ cm}^2$ strips of CH-FP or Cu/CH-FP, 4 ml of 0.012 mM CR aqueous solution and 0.3 ml of 0.1 M NaBH_4 aqueous solution

$$\ln(A_t/A_0) = -kt \quad (4)$$

where k denotes the apparent rate constant. The measured k s for the Cu/CH-FP catalyzed MO and CR reduction reactions were 0.2683 and 0.1655 min^{-1} , respectively.

We can see that the rate constant of the MO reduction reaction was higher than the CR. This could be due to the following reasons. First, the chemical structure of CR is bigger than that of MO. As estimated by Marvin Beans (<https://www.chemaxon.com/>), the van der Waals surface area of CR was 798.19 \AA^3 as compared to MO, which was 426.63 \AA^3 . This makes the CR around twice the size of MO (Figure SI 4). Such a large size of CR may make it difficult to be adsorbed on the catalyst surface. Second, there are two azo groups per molecule of CR as

compared to MO, which has only one. Also, the concentration of CR was slightly higher than the MO concentration during these experiments.

In fact, the catalytic properties of Cu^0 nanoparticles are widely known but their recycling tasks are usually performed by loading them onto substrates (magnetically retrievable) or centrifugation (Chandra et al. 2014; Huang et al. 2008). Even loading onto substrates sometimes requires centrifugation (Zhou et al. 2013). In the present case, the recycling process was easy and just involved pulling the Cu/CH-FP strip from the reaction medium. Figure 9 shows the reduction times for the 75 % degradation of MO and CR during cycles. The reduction times increased when the same Cu/CH-FP strip was utilized, which indicated the lowering of the catalytic performance. Such a decrease in catalytic

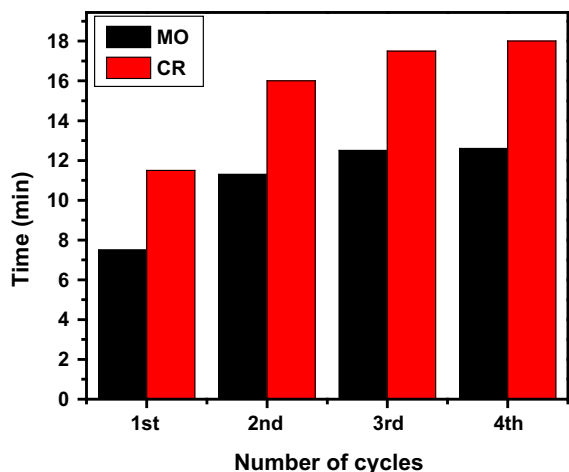


Fig. 9 Time taken by Cu/CH-FP for the 75 % reduction of MO and CR dyes

performance of non-stable transition metal nanoparticles might be due to their oxidation during handling, the slight release of nanoparticles to the solution and aggregation in the swollen polymer layer.

Conclusion

In conclusion, we report a facile approach to synthesizing Cu^0 nanoparticles in the chitosan coating layer over filter paper for catalytic usage. FE-SEM analysis revealed that the nanoparticles were prepared in the chitosan on the cellulose microfibrils of the filter paper. Other properties of the cellulose did not change much during the process as confirmed by the XRD, FTIR and TGA analyses. We showed that Cu/CH-FP could be used to catalyze the reduction reactions of MO and CR by NaBH_4 . The reduction reactions of MO and CR were accomplished within 13 and 17 min, respectively. The Cu/CH-FP was re-used for four times during the reduction reactions of both the dyes where 75 % of the reductions were achieved in less than 20 min. The separation of the Cu/CH-FP was nicely performed by just pulling the strip from the reaction mixture. The developed approach of synthesizing nanoparticles in a thin chitosan layer over filter paper as substrate has great potential for preparing other types of metallic nanoparticles for use in catalytic reactions where easy separation as well as high catalytic performance are required.

Acknowledgments The authors are grateful to the Center of Excellence for Advanced Materials Research (CEAMR) and Chemistry Department at King Abdulaziz University for providing research facilities.

References

- Abidi N, Cabrales L, Haigler CH (2014) Changes in the cell wall and cellulose content of developing cotton fibers investigated by FTIR spectroscopy. *Carbohydr Polym* 100:9–16. doi:[10.1016/j.carbpol.2013.01.074](https://doi.org/10.1016/j.carbpol.2013.01.074)
- Afkhami A, Moosavi R (2010) Adsorptive removal of Congo red, a carcinogenic textile dye, from aqueous solutions by maghemite nanoparticles. *J Hazard Mater* 174:398–403. doi:[10.1016/j.jhazmat.2009.09.066](https://doi.org/10.1016/j.jhazmat.2009.09.066)
- Ahmad A, Syed F, Shah A, Khan Z, Tahir K, Khan AU, Yuan Q (2015) Silver and gold nanoparticles from *Sargentodoxa cuneata*: synthesis, characterization and antileishmanial activity. *RSC Adv* 5:73793–73806. doi:[10.1039/C5RA13206A](https://doi.org/10.1039/C5RA13206A)
- Baig RBN, Varma RS (2013) Magnetically retrievable catalysts for organic synthesis. *Chem Commun* 49:752–770. doi:[10.1039/C2CC35663E](https://doi.org/10.1039/C2CC35663E)
- Caliskan S, Zahmakiran M, Durap F, Ozkar S (2012) Hydrogen liberation from the hydrolytic dehydrogenation of dimethylamine-borane at room temperature by using a novel ruthenium nanocatalyst. *Dalton Trans* 41:4976–4984. doi:[10.1039/C2DT00042C](https://doi.org/10.1039/C2DT00042C)
- Carino EV, Knecht MR, Crooks RM (2009) Quantitative analysis of the stability of pd dendrimer-encapsulated nanoparticles. *Langmuir* 25:10279–10284. doi:[10.1021/la9011108](https://doi.org/10.1021/la9011108)
- Chandra S, Kumar A, Tomar PK (2014) Synthesis and characterization of copper nanoparticles by reducing agent. *J Saudi Chem Soc* 18:149–153. doi:[10.1016/j.jscs.2011.06.009](https://doi.org/10.1016/j.jscs.2011.06.009)
- Chauhan I, Mohanty P (2015) In situ decoration of TiO_2 nanoparticles on the surface of cellulose fibers and study of their photocatalytic and antibacterial activities. *Cellulose* 22:507–519. doi:[10.1007/s10570-014-0480-3](https://doi.org/10.1007/s10570-014-0480-3)
- Chen C-W, Chen M-Q (1998) In situ synthesis and the catalytic properties of platinum colloids on polystyrene microspheres with surface-grafted poly(*N*-isopropylacrylamide). *Chem Commun*. doi:[10.1039/A800203G](https://doi.org/10.1039/A800203G)
- Cordier A, de Resende VG, Weibel A, De Grave E, Peigney A, Laurent C (2010) Catalytic chemical vapor deposition synthesis of double-walled and few-walled carbon nanotubes by using a MoO_3 -supported conditioning catalyst to control the formation of iron catalytic particles within an $\alpha\text{-Al}_2\text{O}_3$ self-supported foam. *J Phys Chem C* 114:19188–19193. doi:[10.1021/jp105712q](https://doi.org/10.1021/jp105712q)
- Datta KKR et al (2014) NZVI modified magnetic filter paper with high redox and catalytic activities for advanced water treatment technologies. *Chem Commun* 50:15673–15676. doi:[10.1039/C4CC06241H](https://doi.org/10.1039/C4CC06241H)
- Dong B, Miller DL, Li CY (2012) Polymer single crystal as magnetically recoverable support for nanocatalysts. *J Phys Chem Lett* 3:1346–1350. doi:[10.1021/jz300434c](https://doi.org/10.1021/jz300434c)
- Eta V, Mikkola J-P (2016) Deconstruction of Nordic hardwood in switchable ionic liquids and acylation of the dissolved

- cellulose. *Carbohydr Polym* 136:459–465. doi:[10.1016/j.carbpol.2015.09.058](https://doi.org/10.1016/j.carbpol.2015.09.058)
- Fihri A, Bouhrara M, Nekouishahraki B, Basset J-M, Polshettiwar V (2011) Nanocatalysts for Suzuki cross-coupling reactions. *Chem Soc Rev* 40:5181–5203. doi:[10.1039/C1CS15079K](https://doi.org/10.1039/C1CS15079K)
- Gautam RK, Rawat V, Banerjee S, Sanroman MA, Soni S, Singh SK, Chattopadhyaya MC (2015) Synthesis of bimetallic Fe–Zn nanoparticles and its application towards adsorptive removal of carcinogenic dye malachite green and Congo red in water. *J Mol Liq* 212:227–236. doi:[10.1016/j.molliq.2015.09.006](https://doi.org/10.1016/j.molliq.2015.09.006)
- Ghodake G, Kim D-Y, Jo JH, Jang J, Lee DS (2016) One-step green synthesis of gold nanoparticles using casein hydrolytic peptides and their anti-cancer assessment using the DU145 cell line. *J Ind Eng Chem* 33:185–189. doi:[10.1016/j.jiec.2015.10.001](https://doi.org/10.1016/j.jiec.2015.10.001)
- González JA, Villanueva ME, Piehl LL, Copello GJ (2015) Development of a chitin/graphene oxide hybrid composite for the removal of pollutant dyes: adsorption and desorption study. *Chem Eng J* 280:41–48. doi:[10.1016/j.cej.2015.05.112](https://doi.org/10.1016/j.cej.2015.05.112)
- Guo Z, Liu B, Zhang Q, Deng W, Wang Y, Yang Y (2014) Recent advances in heterogeneous selective oxidation catalysis for sustainable chemistry. *Chem Soc Rev* 43:3480–3524. doi:[10.1039/C3CS60282F](https://doi.org/10.1039/C3CS60282F)
- Huang Z, Cui F, Kang H, Chen J, Zhang X, Xia C (2008) Highly dispersed silica-supported copper nanoparticles prepared by precipitation – gel method: a simple but efficient and stable catalyst for glycerol hydrogenolysis. *Chem Mater* 20:5090–5099. doi:[10.1021/cm8006233](https://doi.org/10.1021/cm8006233)
- Hudson R, Riviere A, Cirtiu CM, Luska KL, Moores A (2012) Iron-iron oxide core-shell nanoparticles are active and magnetically recyclable olefin and alkyne hydrogenation catalysts in protic and aqueous media. *Chem Commun* 48:3360–3362. doi:[10.1039/C2CC16438H](https://doi.org/10.1039/C2CC16438H)
- Johnson L, Thielemans W, Walsh DA (2011) Synthesis of carbon-supported Pt nanoparticle electrocatalysts using nanocrystalline cellulose as reducing agent. *Green Chem* 13:1686–1693. doi:[10.1039/C0GC00881H](https://doi.org/10.1039/C0GC00881H)
- Kamal T, Ul-Islam M, Khan SB, Asiri AM (2015) Adsorption and photocatalyst assisted dye removal and bactericidal performance of ZnO/chitosan coating layer. *Int J Biol Macromol* 81:584–590. doi:[10.1016/j.ijbiomac.2015.08.060](https://doi.org/10.1016/j.ijbiomac.2015.08.060)
- Khan MM, Lee J, Cho MH (2014a) Au@TiO₂ nanocomposites for the catalytic degradation of methyl orange and methylene blue: an electron relay effect. *J Ind Eng Chem* 20:1584–1590. doi:[10.1016/j.jiec.2013.08.002](https://doi.org/10.1016/j.jiec.2013.08.002)
- Khan SB, Rahman MM, Akhtar K, Asiri AM, Rub MA (2014b) Nitrophenol chemi-sensor and active solar photocatalyst based on spinel hetaerolite nanoparticles. *PLoS ONE* 9:e85290. doi:[10.1371/journal.pone.0085290](https://doi.org/10.1371/journal.pone.0085290)
- Kljun A, Benians TAS, Goubet F, Meulewaeter F, Knox JP, Blackburn RS (2011) Comparative analysis of crystallinity changes in cellulose I polymers using ATR-FTIR, X-ray diffraction, and carbohydrate-binding module probes. *Biomacromolecules* 12:4121–4126. doi:[10.1021/bm201176m](https://doi.org/10.1021/bm201176m)
- Li H, Yang M, Zhang X, Yan L, Li J, Qi Y (2013) Mesoporous silica-supported copper-catalysts for homocoupling reaction of terminal alkynes at room-temperature. *New J Chem* 37:1343–1349. doi:[10.1039/C3NJ41006D](https://doi.org/10.1039/C3NJ41006D)
- Moritz M, Geszke-Moritz M (2013) The newest achievements in synthesis, immobilization and practical applications of antibacterial nanoparticles. *Chem Eng J* 228:596–613. doi:[10.1016/j.cej.2013.05.046](https://doi.org/10.1016/j.cej.2013.05.046)
- Nie Z, Petukhova A, Kumacheva E (2010) Properties and emerging applications of self-assembled structures made from inorganic nanoparticles. *Nat NANO* 5:15–25
- Oh SY et al (2005) Crystalline structure analysis of cellulose treated with sodium hydroxide and carbon dioxide by means of X-ray diffraction and FTIR spectroscopy. *Carbohydr Res* 340:2376–2391. doi:[10.1016/j.carres.2005.08.007](https://doi.org/10.1016/j.carres.2005.08.007)
- Patel R, Suresh S (2006) Decolourization of azo dyes using magnesium–palladium system. *J Hazard Mater* 137:1729–1741. doi:[10.1016/j.jhazmat.2006.05.019](https://doi.org/10.1016/j.jhazmat.2006.05.019)
- Pezzato C, Maiti S, Chen JLY, Cazzolaro A, Gobbo C, Prins LJ (2015) Monolayer protected gold nanoparticles with metal-ion binding sites: functional systems for chemosensing applications. *Chem Commun* 51:9922–9931. doi:[10.1039/C5CC00814J](https://doi.org/10.1039/C5CC00814J)
- Plum A, Braun G, Rehorek A (2003) Process monitoring of anaerobic azo dye degradation by high-performance liquid chromatography–diode array detection continuously coupled to membrane filtration sampling modules. *J Chromatogr A* 987:395–402. doi:[10.1016/S0021-9673\(02\)01906-4](https://doi.org/10.1016/S0021-9673(02)01906-4)
- Rehman S, Siddiq M, Al-Lohedan H, Sahiner N (2015) Cationic microgels embedding metal nanoparticles in the reduction of dyes and nitro-phenols. *Chem Eng J* 265:201–209. doi:[10.1016/j.cej.2014.12.061](https://doi.org/10.1016/j.cej.2014.12.061)
- Sahiner N (2013) Soft and flexible hydrogel templates of different sizes and various functionalities for metal nanoparticle preparation and their use in catalysis. *Prog Polym Sci* 38:1329–1356. doi:[10.1016/j.progpolymsci.2013.06.004](https://doi.org/10.1016/j.progpolymsci.2013.06.004)
- Sahiner N, Ozay H, Ozay O, Aktas N (2010) A soft hydrogel reactor for cobalt nanoparticle preparation and use in the reduction of nitrophenols. *Appl Catal B Environ* 101:137–143. doi:[10.1016/j.apcatb.2010.09.022](https://doi.org/10.1016/j.apcatb.2010.09.022)
- Sahiner N, Ozay O, Inger E, Aktas N (2011) Superabsorbent hydrogels for cobalt nanoparticle synthesis and hydrogen production from hydrolysis of sodium boron hydride. *Appl Catal B* 102:201–206. doi:[10.1016/j.apcatb.2010.11.042](https://doi.org/10.1016/j.apcatb.2010.11.042)
- Sapsford KE et al (2013) Functionalizing nanoparticles with biological molecules: developing chemistries that facilitate nanotechnology. *Chem Rev* 113:1904–2074. doi:[10.1021/cr300143v](https://doi.org/10.1021/cr300143v)
- Sarkar B, Pendem C, Konathala LNS, Sasaki T, Bal R (2014) Pt nanoparticle supported on nanocrystalline CeO₂: highly selective catalyst for upgradation of phenolic derivatives present in bio-oil. *J Mater Chem A* 2:18398–18404. doi:[10.1039/C4TA04542D](https://doi.org/10.1039/C4TA04542D)
- Shen J, Yin X, Karpuzov D, Semagina N (2013) PVP-stabilized mono- and bimetallic Ru nanoparticles for selective ring opening. *Catal Sci Technol* 3:208–221. doi:[10.1039/C2CY20443F](https://doi.org/10.1039/C2CY20443F)
- Smuleac V, Varma R, Sikdar S, Bhattacharyya D (2011) Green synthesis of Fe and Fe/Pd bimetallic nanoparticles in membranes for reductive degradation of chlorinated organics. *J Membr Sci* 379:131–137. doi:[10.1016/j.memsci.2011.05.054](https://doi.org/10.1016/j.memsci.2011.05.054)
- Song D, Yi W-B (2008) Polymethyl methacrylate micro-spheres supported palladium: a new catalyst for Heck and Suzuki

- reactions. *J Mol Catal A: Chem* 280:20–23. doi:[10.1016/j.molcata.2007.10.017](https://doi.org/10.1016/j.molcata.2007.10.017)
- Xiao S, Xu W, Ma H, Fang X (2012) Size-tunable Ag nanoparticles immobilized in electrospun nanofibers: synthesis, characterization, and application for catalytic reduction of 4-nitrophenol. *RSC Adv* 2:319–327. doi:[10.1039/C1RA00127B](https://doi.org/10.1039/C1RA00127B)
- Yan W, Chen B, Mahurin SM, Dai S, Overbury SH (2004) Brookite-supported highly stable gold catalytic system for CO oxidation. *Chem Commun*. doi:[10.1039/B405434B](https://doi.org/10.1039/B405434B)
- Zahmakran M, Ozkar S (2011) Metal nanoparticles in liquid phase catalysis; from recent advances to future goals. *Nanoscale* 3:3462–3481. doi:[10.1039/C1NR10201J](https://doi.org/10.1039/C1NR10201J)
- Zhang Q, Deng W, Wang Y (2011) Effect of size of catalytically active phases in the dehydrogenation of alcohols and the challenging selective oxidation of hydrocarbons. *Chem Commun* 47:9275–9292. doi:[10.1039/C1CC11723H](https://doi.org/10.1039/C1CC11723H)
- Zheng G, Polavarapu L, Liz-Marzan LM, Pastoriza-Santos I, Perez-Juste J (2015) Gold nanoparticle-loaded filter paper: a recyclable dip-catalyst for real-time reaction monitoring by surface enhanced Raman scattering. *Chem Commun* 51:4572–4575. doi:[10.1039/C4CC09466B](https://doi.org/10.1039/C4CC09466B)
- Zhong C, Wang C, Wang F, Jia H, Wei P, Zhao Y (2016) Application of tetra-*n*-methylammonium hydroxide on cellulose dissolution and isolation from sugarcane bagasse. *Carbohydr Polym* 136:979–987. doi:[10.1016/j.carbpol.2015.10.001](https://doi.org/10.1016/j.carbpol.2015.10.001)
- Zhou Z, Lu C, Wu X, Zhang X (2013) Cellulose nanocrystals as a novel support for CuO nanoparticles catalysts: facile synthesis and their application to 4-nitrophenol reduction. *RSC Adv* 3:26066–26073. doi:[10.1039/C3RA43006E](https://doi.org/10.1039/C3RA43006E)